A.

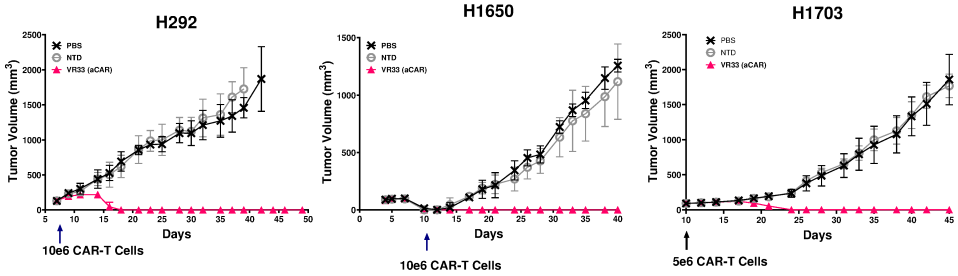

B.

CAR Target	Sites Cell
HER2	1.5E4
HLA-A2	0

CAR Target	Sites Cell
HER2	2.8E4
HLA-A2	1.0E6

CAR Target	Sites Cell
HER2	2.0E4
HLA-A2	8.0E5

C.

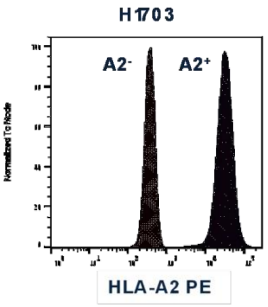

D.

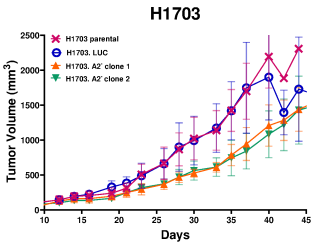

Supplemental Figure S1. A second generation HER2 targeted aCAR eradicates lung tumors expressing low/normal HER2. (A) NSG mice (NOD.Cg-Prkdcscid Il2rgtm1Wjl/SzJ) were implanted subcutaneously with 5E6 tumor cells in 50% matrigel and dosed with 10E6 of VR33 aCAR-T cells (i.v.). Tumor growth was monitored 3x per week. The study was terminated when tumor size reached 2000 mm^3 in control groups. (B) iCAR and aCAR antigen expression level in lung cancer cells. The per cell concentration of A2 and HER2 in cell culture listed under each tumor model was determined by quantitative FACS (qFACS) as described in **online Supplemental Table S2**. (C) FACS analysis of $A2^+$ and CRISPR edited $A2^-$ H1703 cell lines. H1703 lung cancer cells representing A2 LOH were generated by CRISPR editing of cells expressing firefly luciferase. A2 editing was verified by FACS analysis using a PE-labeled anti HLA-A2 BB7.2 antibody and Illumina genomic sequencing. (D) *In-vivo* growth rate of H1703-$A2^+$ and $A2^-$ tumors. The growth rates of $A2^+$ and $A2^-$ H1703 tumors were characterized in NSG mice as described in (A) for PBS controls.

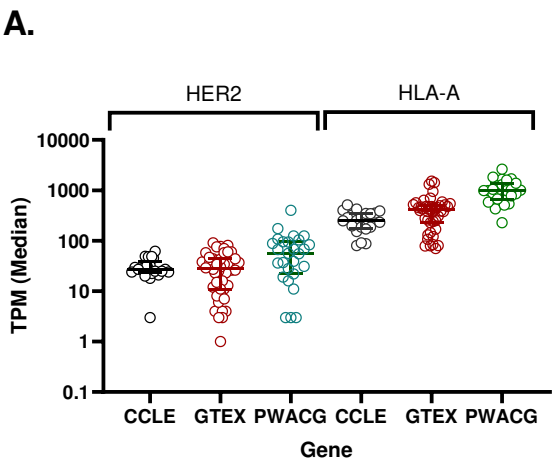

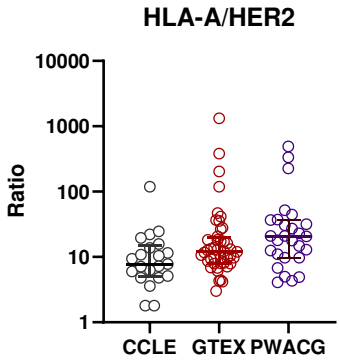

C.

Column Statistics	HER2 (TPM)			HLA-A (TPM)			HLA-A/HER2 Ratio		
	CCLE	GTEX	PWACG	CCLE	GTEX	PWACG	CCLE	GTEX	PWACG
Min	18	3	3	80	70	228	2	3	4
25th percentile	24	12	30	182	231	631	5	8	10
Median	27	30	68	251	410	990	7	12	18
75th percentile	35	44	97	344	481	1313	12	18	31
Max	62	91	400	516	1427	2623	25	204	335
Mean	32	33	81	261	393	1042	10	21	20
Std Dev	12	24	80	120	254	548	7	35	13

Supplemental Figure S2. Similar range of A2 and HER2 RNA expression in cell-lines, normal tissues and tumors. (A) Median RNA expression frequency distribution. The median expression of HER2 and HLA-A in each CCLE histological type, GTEX normal tissues, and a panel of PWACG tumors was plotted as a frequency histogram. (B) Expression ratios. The ratio of HLA-A to HER2 (HLA-A/HER2) expression for the samples represented in (A) were represented as a frequency histogram. The outliers with ratio > 100 are hematopoietic samples in which HER2 expression is near baseline detection. (C) Descriptive statistics. The table lists column statistics describing the RNAseq data represented in (A,B). Hematopoietic samples were omitted. The HLA-A/HER2 ratio across the three data sets is similar (17±6). RNAseq data was accessed through Expression Atlas (https://www.ebi.ac.uk/gxa/home) [1–3]

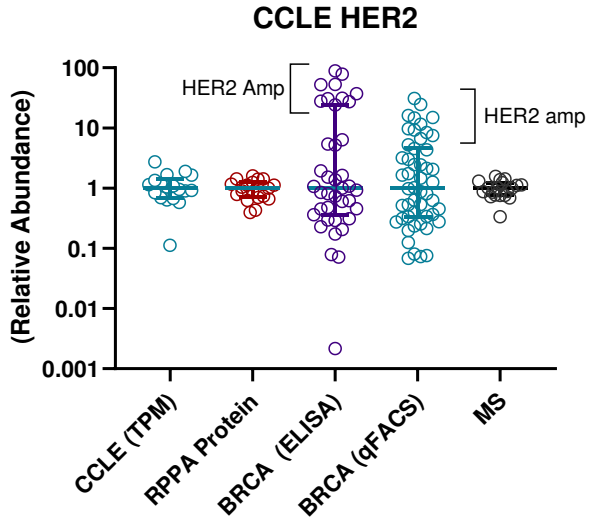

Supplemental Figure S3. Comparison of RNAseq and HER2 protein expression. HER2 protein expression data was collected from several different sources: RPPA Protein[4], BRCA ELISA[5], BRCA1 quantitative (q)FACS (Dennis J. Slamon; UCLA, personal communication), and mass spectrometry MS[6]. The HER2 expression values in the RPPA and MS proteomic data are the median for each histological type to avoid tissue bias. The breast cancer (BRCA) frequency plots represent individual cancer cell lines in which absolute protein concentrations were determined by ELISA or qFACS. Amplified HER2 by qFACS ranged from about 10E4 to 10E5 receptors per cell (median, 3.0E5 per cell), while low/normal expression ranges from about 2.0E3 to 5.0E4 per cell (median 1.1E4 per cell). The ELISA estimates of HER2 in total protein extracts and qFACS measurements are reasonably well correlated in log-log comparisons (Pearson Correlation Coefficient 0.77, data not shown), but ELISA values exceeding qFACs by about 3-fold. Relative protein estimates of HER2 and other receptor tyrosine kinases obtained using quantitative expression profiling (MS) in a large set of CCLE cell-lines are significantly correlated with RPKM data (Pearson Correlation Coefficient 0.7-0.8)[6]. We have obtained similar correlations for HER2 protein determined by RPPA, ELISA and qFACS versus RNAseq (data not shown). Standard curves, derived from the log-plot of TPM against qFACS breast cancer cell line data, was used to interpolate HER2 concentration (receptors per cell) from the median TPM: CCLE, 1.1E4; GTEX, 1.2E4; PWACG 2.3E4. The protein measurements to support a similar calibration for HLA-A were based soley on the A2 qFACS measurements in **online Supplemental Table S2**, since RPPA and MS proteomics were not available due to high protein polymorphism: CCLE, 5.3E5; GTEX 7.4E5; PWACG, 1.3E6 median HLA-A per cell.

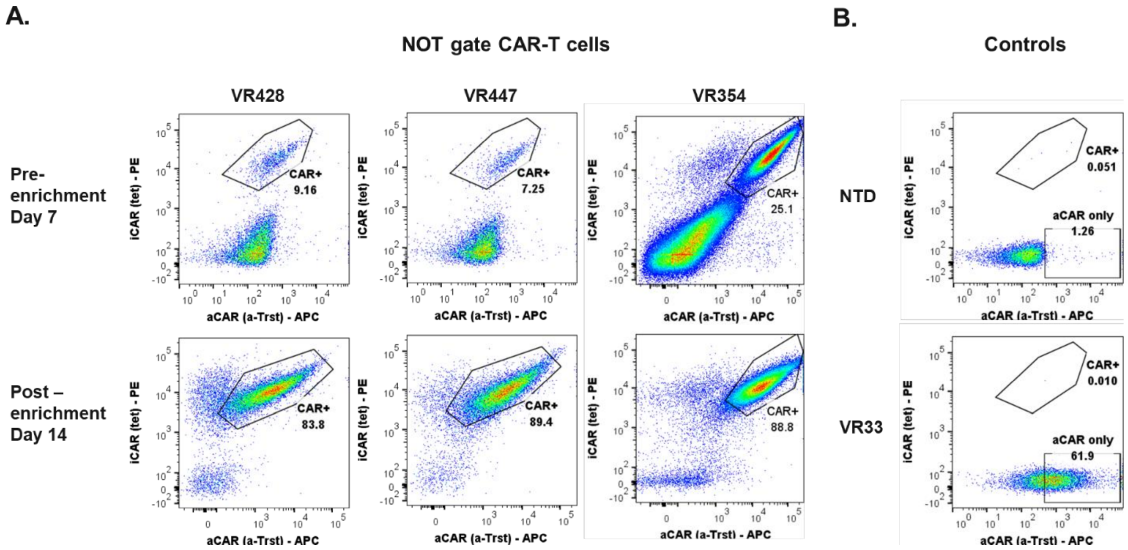

Supplemental Figure S4. Enrichment of NOT gate CAR-T cells and mock control process. (A) NOT gate CAR enriched cells. The transduction efficiency of T cells with NOT gate lentiviral constructs ranged from about 5% to 35% CAR positive across all LIR1 iCAR candidates tested. NOT gate CAR-T cells were enriched by capture with A2 PE-labeled tetramers on day 7 post transduction, to eliminate assay variability associated with transduction efficiency. Enriched cells were reactivated using 1:100 TransAct in 1ml culture medium. On day 8, 6ml of culture media were added, followed by IL2 replenishment (day 10 or 11), culture medium replacement (day 12). The purity of NOT gate CAR positive cells increased during the expansion leading up to harvesting on day 14. (B) Mock enriched controls. NTD and VR33 aCAR-T cells were treated the same in parallel except iCAR capture was omitted.

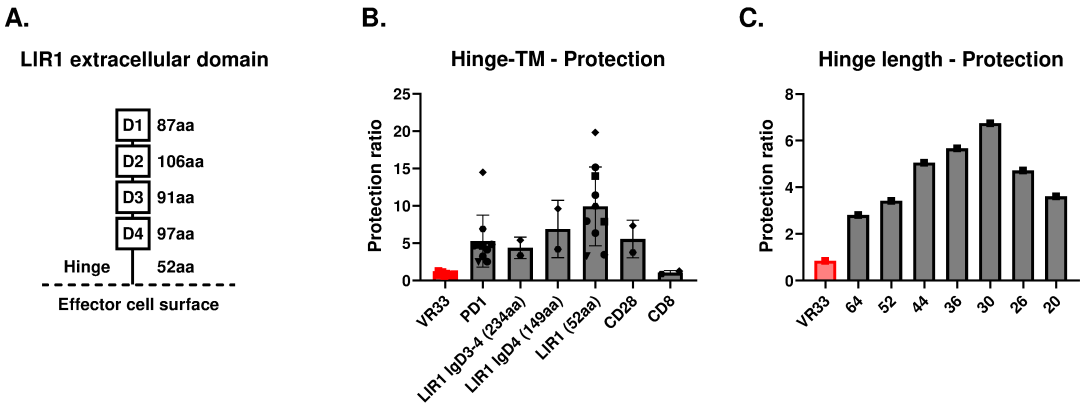

Supplemental Figure S5. Hinge-transmembrane (HTM) optimization. (A) Structure of the LIR1 extracellular domain (ECD). The LIR1 extracellular region consists of four Ig-like domains (D1-D4) of 433 total residues followed by a 52 amino acid juxtamembrane stem. The N-terminal D1 and D2 motifs are responsible for binding HLA-A complex [8]. (B) D1-D4 deletion series. Ig-motif deletions were incorporated into an iCAR backbone as indicated and killing assays were performed to evaluate the effect on protection and efficacy. A CD28 HTM (66 residues, hinge 39) functioned as well as the VR51 PD1 HTM (VR51), but protection was lost with a CD8a HTM (69 residues, hinge 45). The protection ratio is equal to $A2^{+}_{EC50}/A2^{-}_{EC50}$. Each data point represents an independent measurement. The designated donor PBMC symbol for each CAR-T preparation is consistent across the **Results**. (C) High resolution hinge deletion. The optimal hinge length was determined by higher resolution deletion mapping.

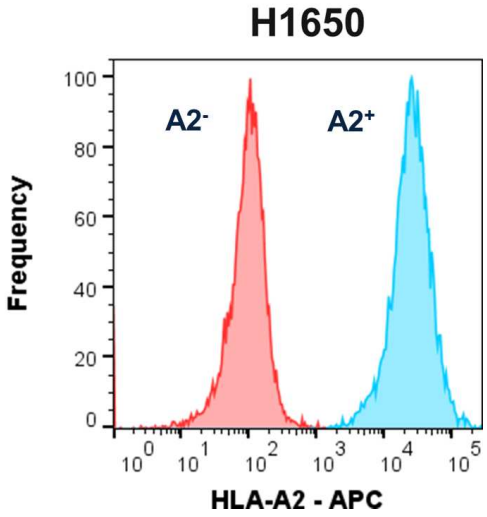

Supplemental Figure S6. FACS analysis of H1650-A2$^+$ and A2$^-$ target cells. H1650 A2$^-$ cells were generated by CRISPR editing as described in **Methods** and confirmed by FACS with anti HLA-A2 antibody (BB7.2).

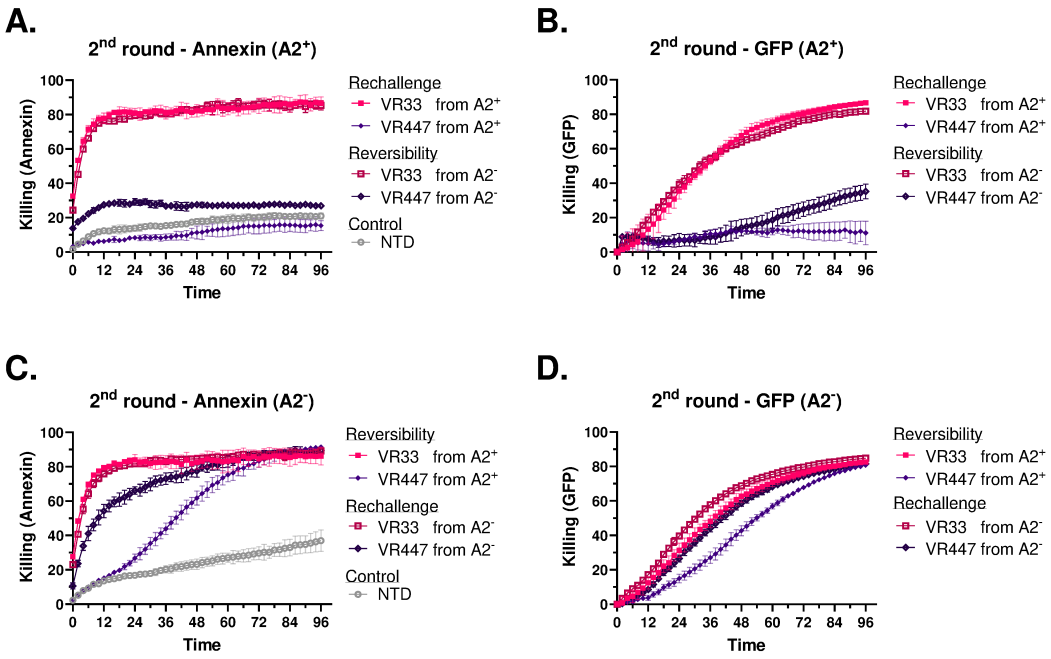

Supplemental Figure S7. Antigen exchange and repeated challenge assays at higher E:T ratio. CAR-T cells were preincubated with target cells (E:T 1.5:1) for 48 h. Targets were then enriched by anti E-cadherin and P-cadherin antibody selection. The purified cells were applied to either H1650-A2$^+$ or H1650-A2$^-$ targets (E:T 3:1). Target killing (Annexin V) or growth inhibition was monitored by Incucyte imaging. (A,B) H1650-A2$^+$ rechallenge assays. The CAR-T cell pretreatment condition is indicated in the legend. NTD cells were not pretreated. (A) Annexin V readout. (B) Cell growth inhibition. The change in GFP$^+$ cell area was normalized to the T_0 value and NTD. (C,D) H1650-A2$^-$ rechallenge assay. The rechallenge to test durability was performed as described for (A,B) except the targets were H1650-A2$^-$ cells.

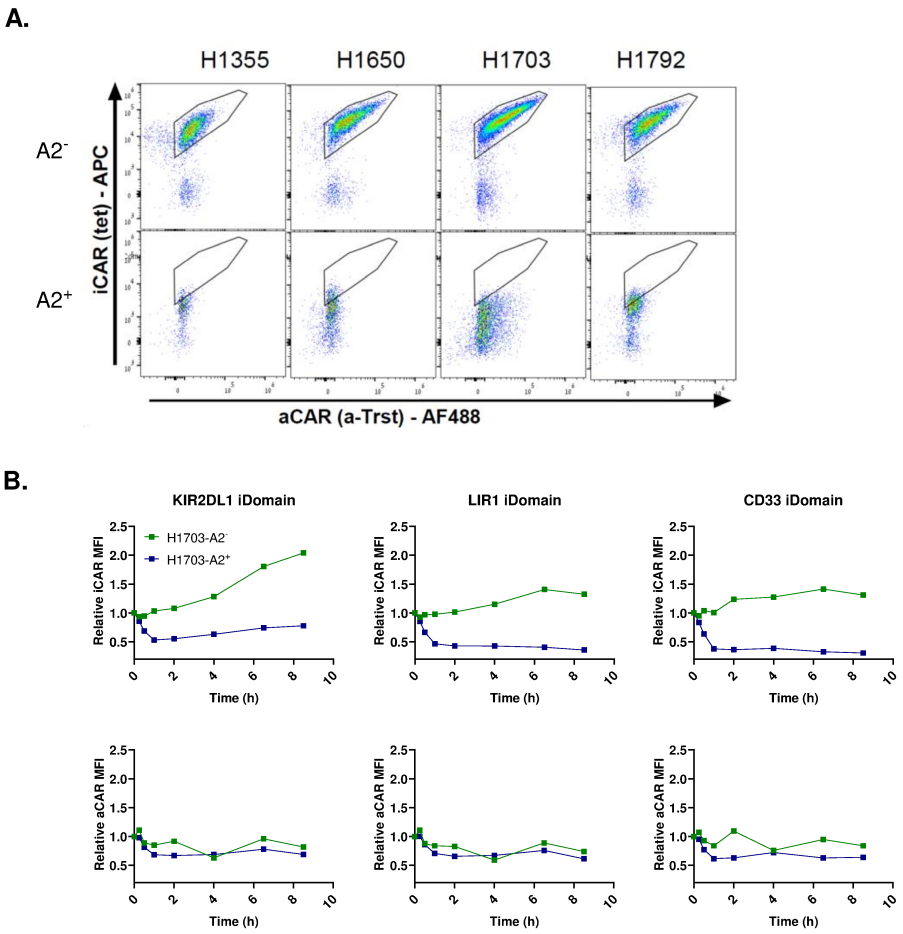

Supplemental Figure S8. CAR internalization kinetics. (A) FACS plots of aCAR and iCAR surface expression. VR354 CAR-T cells were co-cultured for 18 h with $A2^+$ or $A2^-$ lung cancer cell lines and profiled for aCAR and iCAR surface expression. The target levels on each lung cancer cell line are listed in **online Supplemental Table S2.** (B) Time course of CAR downregulation. The change in iCAR and aCAR cell-surface levels relative to effector only were followed by FACS analysis as described in (A) for VR49 (KIR2DL1 iDomain), VR51 (LIR1 iDomain) and VR54 (CD33 iDomain) CAR-T cells. Exposure to H1703-$A2^+$ lung cancer cells reduced iCAR and aCAR surface expression within about 1 h; whereas iCAR and aCAR expression tended to increase following exposure to H1703-$A2^-$ cells.

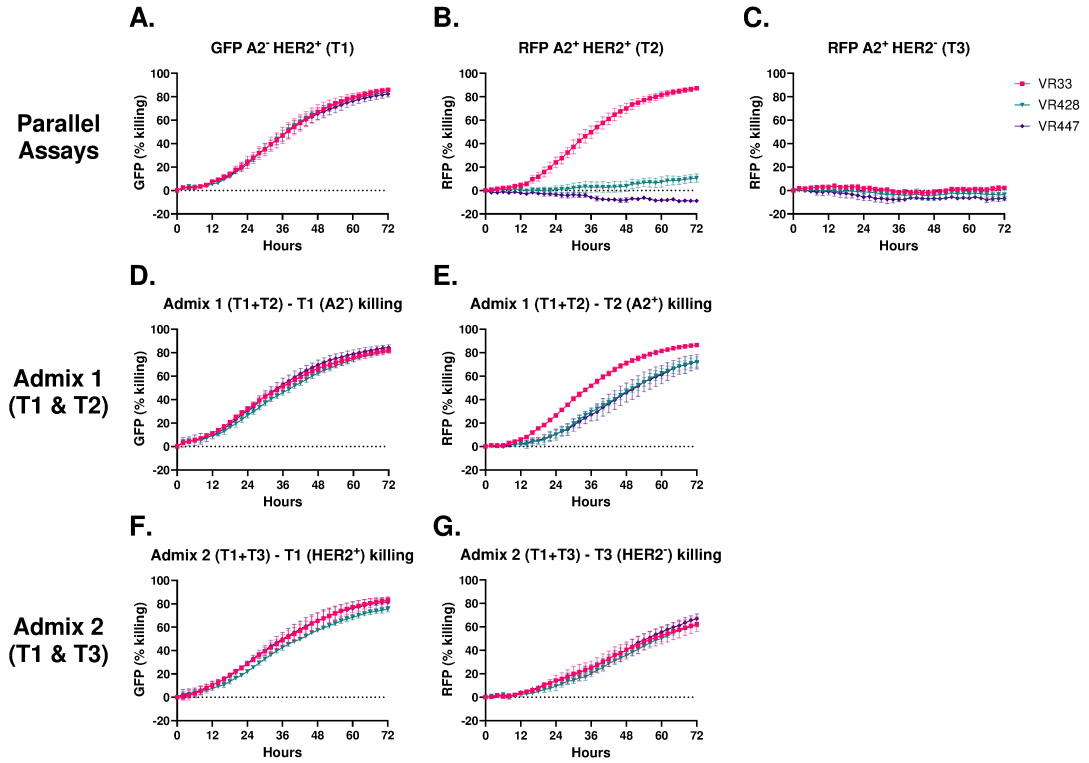

Supplemental Figure S9. Evaluation of the A2 and HER2 dependence of target cell killing in parallel and admix cultures. (A-C) Parallel Assays. GFP labeled H1650-$A2^-$ $HER2^+$ cells and RFP labeled H1650 $A2^+$ $HER2^+$ or $A2^-$ $HER2^-$ cells were separately treated with CAR-T cells (E:T 4:1). GFP and RFP integrated total fluorescence intensity was viably monitored using an Incucyte platform. Growth for each treatment was normalized to T_0. The % killing expressed the growth inhibition in the treated wells relative to the NTD control. The AUC shown in **Figure 5C** was derived from these kinetic plots. The killing kinetics of GFP $A2^-$ $HER2^+$ targets was unaffected by the presence of RFP $A2^+$ $HER2^+$ targets in admix cultures (compare A to D,F). The HER2 targeted bystander killing of RFP $A2^+$ $HER2^+$ targets in admix cultures occurs at a reduced rate compared to VR33 aCAR-T controls and GFP $A2^-$ $HER2^+$ in parallel assays (compare D and E). Nonspecific bystander killing of RFP $A2^+$ $HER2^-$ targets in admix cultures occurs at a lower rate compared to bystander killing of RFP $A2^+$ $HER2^+$ targets (compare E and G). The HER2 independent killing kinetics of VR33 aCAR-T and NOT gate CAR-T cells were indistinguishable.

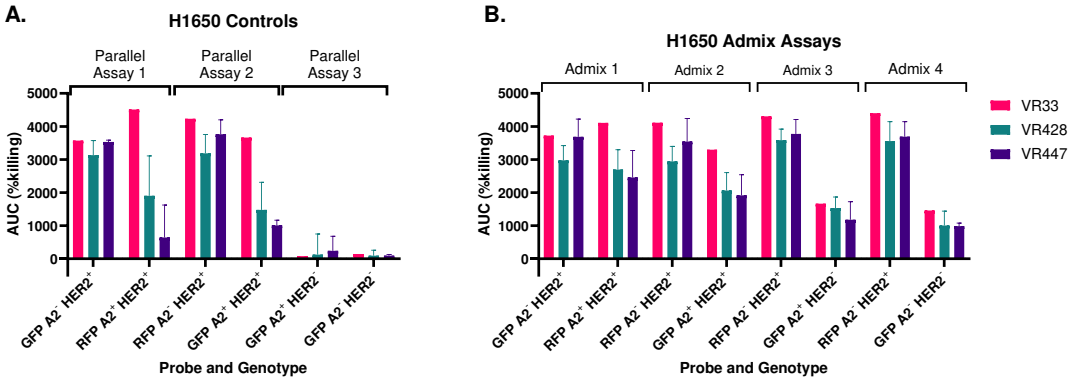

Supplemental Figure S10. Replication of the HER2 dependent and HER2 independent bystander effects. The experiment shown in **Figure 5C,D** and **online Supplemental Figure S9** was repeated (E:T 4:1) to rule out technical artifacts related to the detection or expression of fluorescent proteins. The results were generated with a single preparation of VR33 aCAR-T cells. The error bars shown for NOT gate CAR-T cells represent the variability seen with two different test article preparations in assays performed at the same time. (A) Parallel control assays. Swapping GFP and RFP labels does not significantly alter the selectivity of CAR-T cells test articles. (Compare Parallel Assays 1 and 2). Parallel Assay 3 was included to demonstrate that iCAR activity (A2 expression) does not alter the dependence of VR33 aCAR-T targeted killing on HER2 expression in parallel assays. (B) Admix assays. The HER2 dependent bystander effect is not influenced by fluorescent protein labeling (compare Admix 1 and Admix 2). Nonspecific, HER2 independent bystander killing is not significantly affected by iCAR engagement (compare Admix 3 and Admix 4).

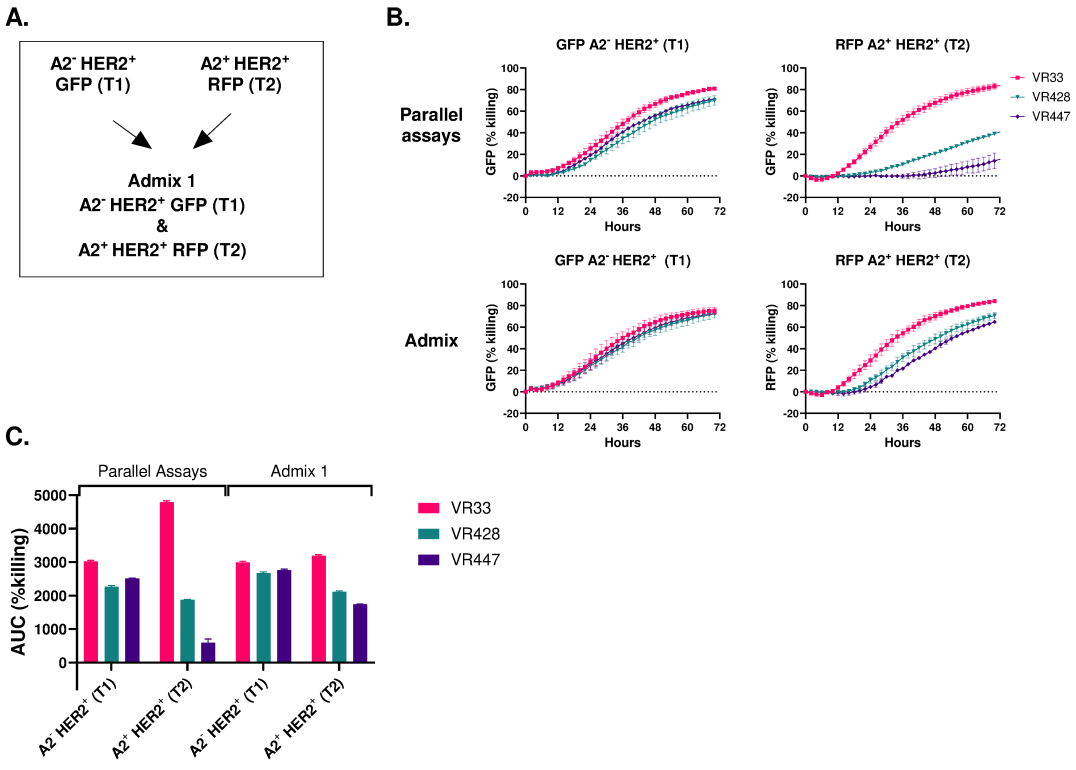

Supplemental Figure S11. Bystander activity is not cell-line specific. (A) Assay design. The 2D parallel and admix experiments described in **Figure 5C** were repeated using H1703 lung cancer cells as targets: (T1) GFP A2⁻ HER2⁺ and (T2) RFP A2⁺ HER2⁺. (B) Killing Kinetics. The effect of the indicated CAR-T test articles was monitored by viably imaging of total fluorescent intensity. (C) AUC killing. The AUC for killing (T_0 to T72 $_h$) was derived from the kinetic data shown in (B).

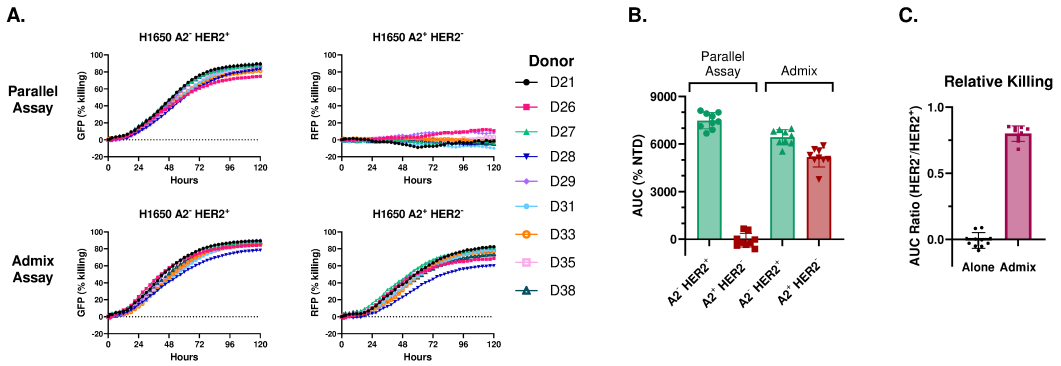

Supplemental Figure S12. The HER2 independent bystander effect was replicated with multiple donors. (A) VR33 aCAR-T cells were prepared from nine different PBMC donors. GFP H1650-A2$^-$HER2$^+$ and RFP H1650-A2$^+$ HER2$^-$ target cells were treated in either separate (Parallel Assays) or mixed (Admix) cultures (E:T 4:1). The effect on target growth was followed by monitoring total fluorescence intensity using an Incucyte platform. (B) AUC of target killing. The AUC from T_0 to T_{120} as derived from the killing curves shown in A. CAR-T cell killing was highly dependent on HER2 expression in parallel assays, but this selectivity was greatly reduced in admix culture. (C) Selectivity Ratio. The killing specificity of was expressed as the AUC ratio of A2$^-$ HER$^+$ over A2$^+$ HER2$^-$ targets. The ratio equaled 0.80 $\pm$ 0.05.

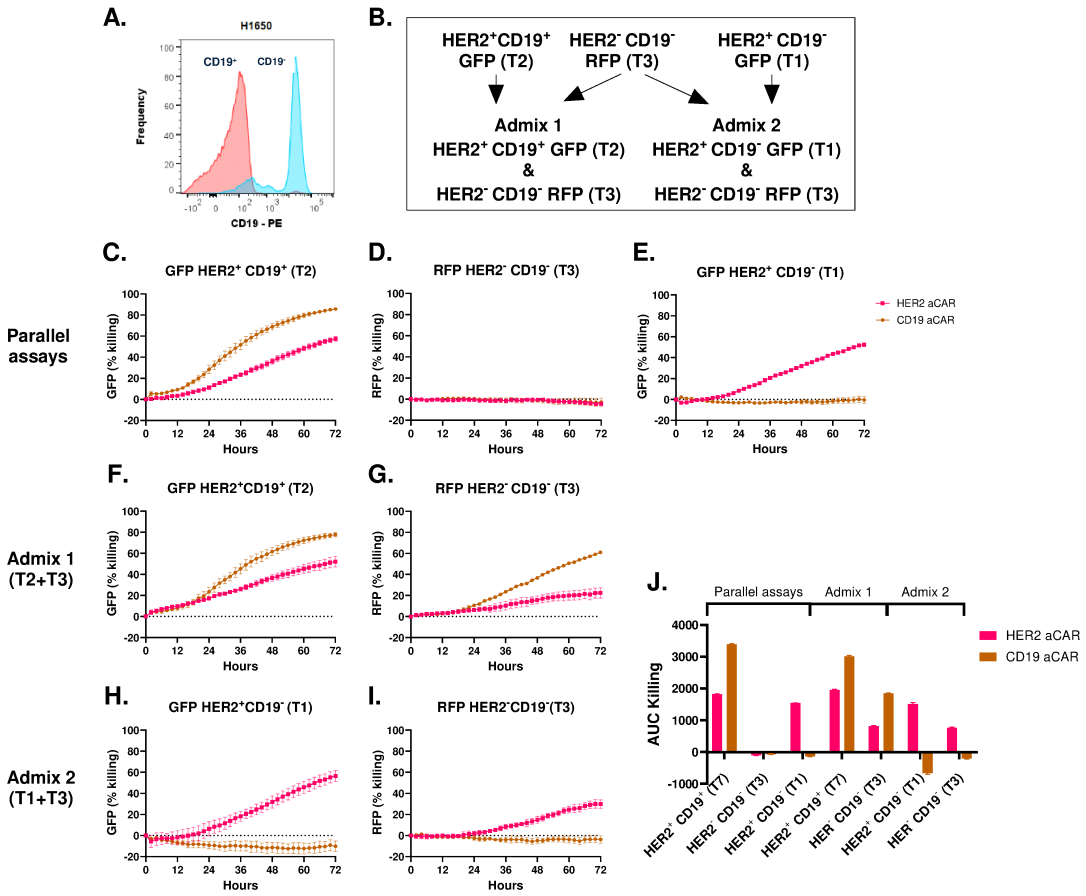

Supplemental Figure S13. The bystander effect is not peculiar to a HER2 aCAR. Admix assays were performed with a second generation CD19 aCAR that includes the same 4-1BB costimulatory region and CD3ζ domain as the VR33 aCAR. H1650 lung cancer cells are CD19 negative ($CD19^-$). GFP labeled CD19 positive ($CD19^+$) H1650 cells were engineered to transgenically express the full-length CD19. (A) Confirmation of CD19 expression. CD19 expression was examined by FACS analysis using anti CD19-PE labeled antibody. (B) Design of parallel controls and admix experiments. (C-E) Parallel control killing kinetics. $HER2^+$ $CD19^-$ (T1), GFP labeled $HER2^+$ $CD19^+$ (T2), and RFP labeled $HER2^-$ $CD19^-$ (T3) target cells were individually treated with CD19 aCAR-T or VR33 aCAR-T cells (E:T 4:1) and total fluorescent intensity was monitored for 72 h. The CD19 aCAR -T cell growth inhibition was specific for the $CD19^+$ targets (compare C and E). The VR33 aCAR-T cells killed regardless of CD19 status except when HER2 expression was deleted by CRISPR editing. (F-I) Admix assays. The dependence of the CD19 aCAR-T cell killing on CD19 target expression, and the dependence of the VR33 aCAR-T cell killing on HER2 expression is lost in admix

assays including double negative targets (Admix 1, F,G). The loss of VR33 aCAR-T cell target specificity in this admix experiment was not influenced by CD19 expression (Admix 2, H,I). (J) AUC killing histogram. The AUC for target killing was derived for the killing curves shown in C-I. The potency of target independent bystander effects is reduced by 40% to 60% relative to specific killing, consistent with the results presented in **Figure 5C**,**D** and **online Supplemental Figure S10**.

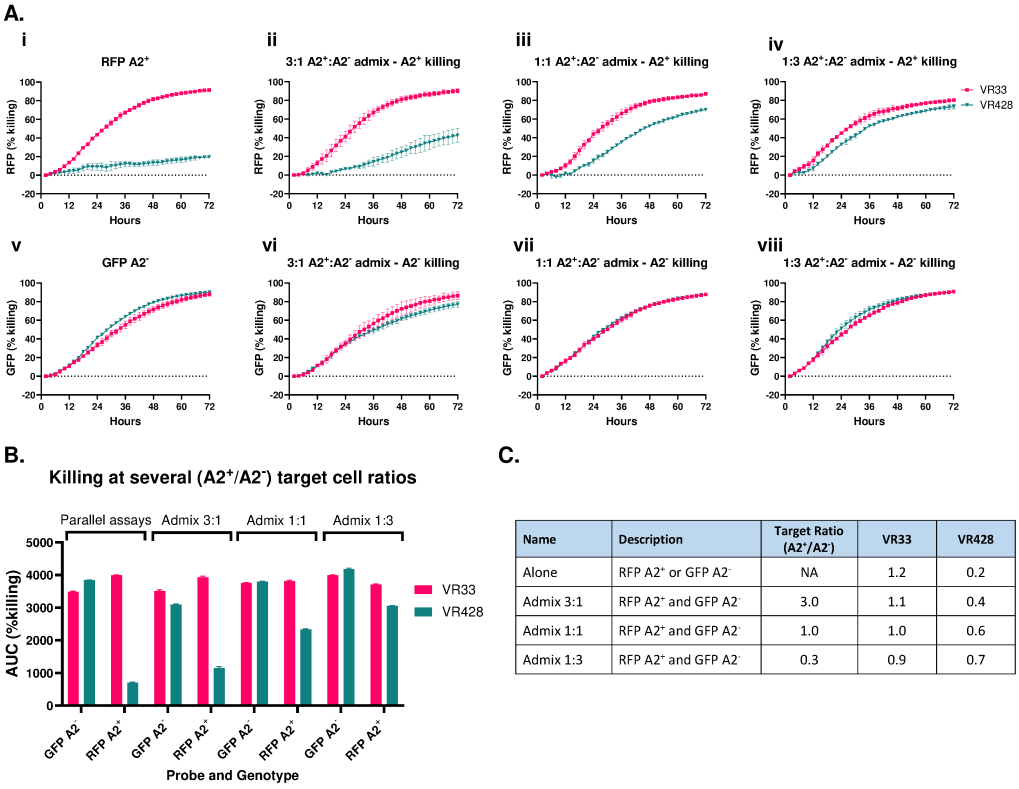

Name	Description	Target Ratio ($A2^+/A2^-$)	VR33	VR428
Alone	RFP $A2^+$ or GFP $A2^-$	NA	1.2	0.2
Admix 3:1	RFP $A2^+$ and GFP $A2^-$	3.0	1.1	0.4
Admix 1:1	RFP $A2^+$ and GFP $A2^-$	1.0	1.0	0.6
Admix 1:3	RFP $A2^+$ and GFP $A2^-$	0.3	0.9	0.7

Supplemental Figure S14. The rate and extent of $A2^+$ target killing in admix cultures is sensitive to the $A2^+/A2^-$ target cells ratio. The specificity of CAR-T cells killing in admix cultures at several H1650 $A2^+/A2^-$ target ratios (3:1, 1:1 and 1:3) was examined at (E:T 4:1 overall). (Ai). $A2^+$ target cell killing control. RFP $A2^+$ $HER2^+$ target cells were separately treated. (Aii-iv). Admix assays. RFP $A2^+$ $HER2^+$ target cell killing kinetics at different target ratios. (Av). $A2^-$ target cell killing control. GFP $A2^-$ $HER2^+$ target cells were separately treated. A(vi-viii). Admix assays. GFP $A2^-$ $HER2^+$ target cell killing kinetics at different target ratios. (B) Histogram of AUC for killing kinetics (A). (C) Tabular summary. The AUC obtained for $A2^+$ and $A2^-$ target cell killing was expressed as a ratio ($A2^+/A2^-$). The protection of $A2^+$ target moderately increases at higher ($A2^+/A2^-$) ratios. The activity of VR33 aCAR-T cells was consistent at all ratios.

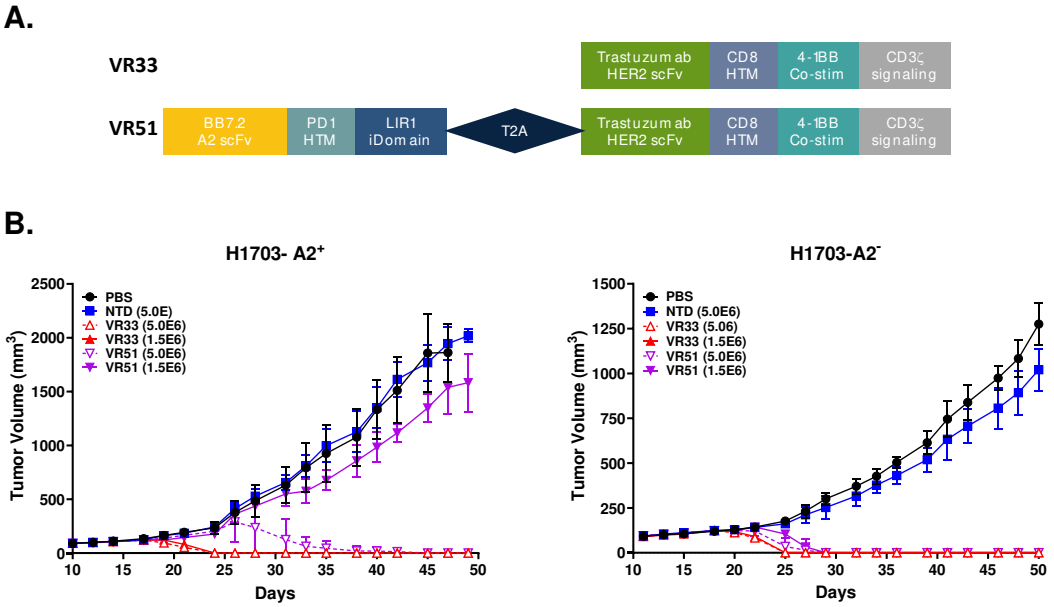

Supplemental Figure S15. VR51 CAR-T cells protect A2$^+$ lung tumors. (A) Structure of VR51 NOT gate construct and VR33 control. (B) H1703-A2$^+$ or H1703-A2$^-$ cells were subcutaneously implanted into NSG mice and intravenously treated with CAR-T cells 10 to 11 days later. With this iteration of NOT gate construct design, protection of H1703-A2$^+$ tumor was observed at the lower 1.5E6 CAR-T cell group, but not at higher 5E6 CAR-T cell group. The H1703-A2$^+$ tumor control was delayed by about 1-2 weeks, but tumor was fully eliminated by day 40. Results are the mean (± S.D) tumor volumes of 5 individual mice.

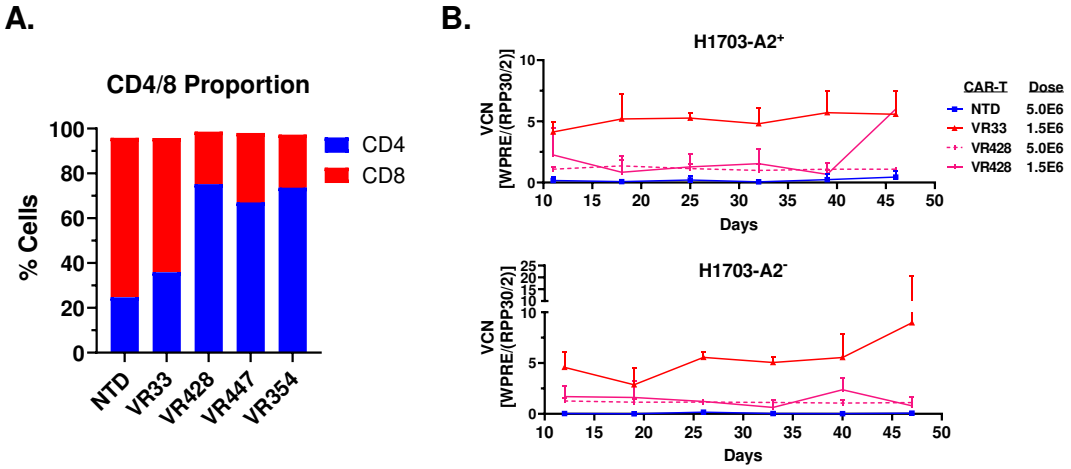

Supplemental Figure S16. CAR-T phenotype and Vector Copy Number (VCN). (A) Proportion of $CD4^+$ and $CD8^+$ CAR-T was measured for each test article using flow cytometry. Representative results from >3 preparations. (B) VCN was evaluated in whole blood at the indicated sampling points following injection to H1703 tumor bearing mice. Upon plasma collection, DNA was isolated from the remaining cell pellets using a MagMAX DNA multi-sample Ultra 2.0 kit on the KingFisher Flex (n = 5 per group). VCN was calculated as the relative ratio of woodchuck hepatitis virus post-transcriptional regulatory element (WPRE), included in the 3' UTR of each lentivirus evaluated, to RPP30 ribonuclease P/MRP subunit p30 (RPP30), a reference gene stably expressed in human cells.

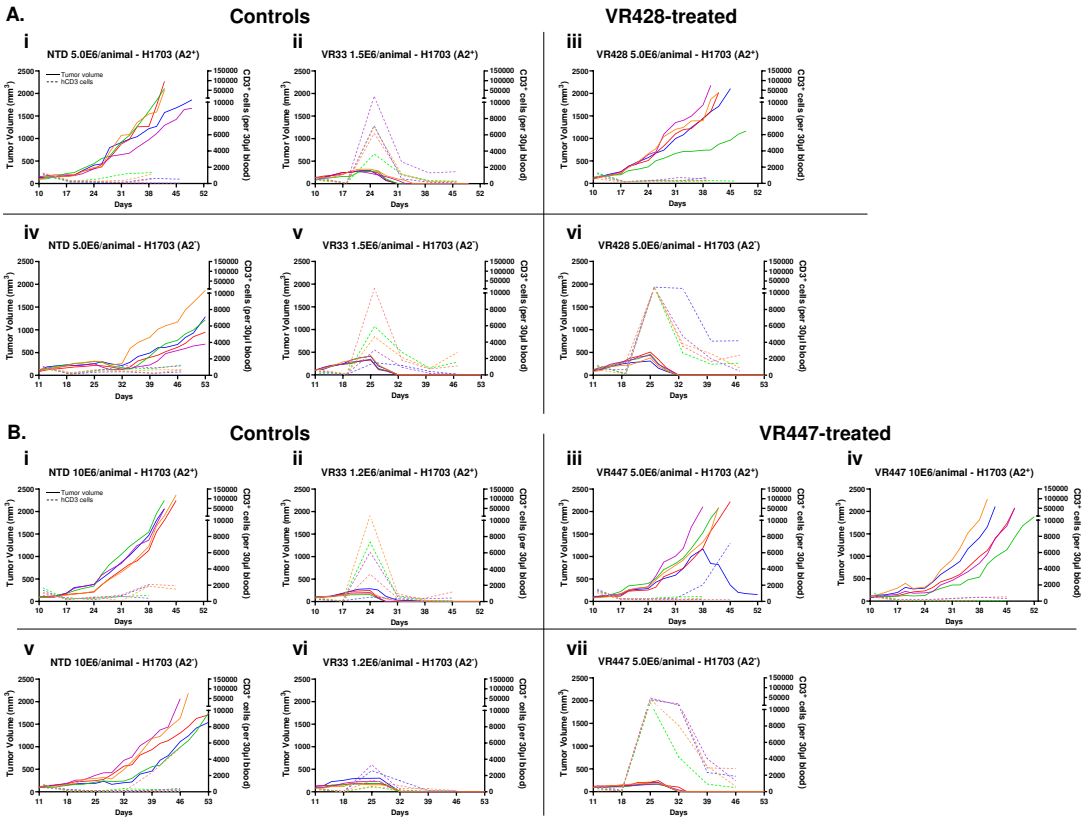

Supplemental Figure S17. NOT gate CAR-T engagement inhibits CAR-T cell expansion *in-vivo*. (A,B) Correlation of tumor growth inhibition and hCD3$^+$ T-cell amplification. Mice bearing H1703 A2$^+$ or A2$^-$ tumors were treated with VR33, VR428 or VR447 transduced CAR-T cells or NTD T-cells as indicated. Tumor volumes measurements (3x/week) and hCD3$^+$ T-cell counts (1x/week) taken for individual mice are color coded in each plot (solid line, tumor volume ; dash line, hCD3$^+$ counts). Potent tumor control typically occurred on about Day 25 and was strongly correlated with CAR-T cell amplification. Delayed sporadic loss of protection in NOT gate CAR-T treated mice was also associated with T-cell expansion.

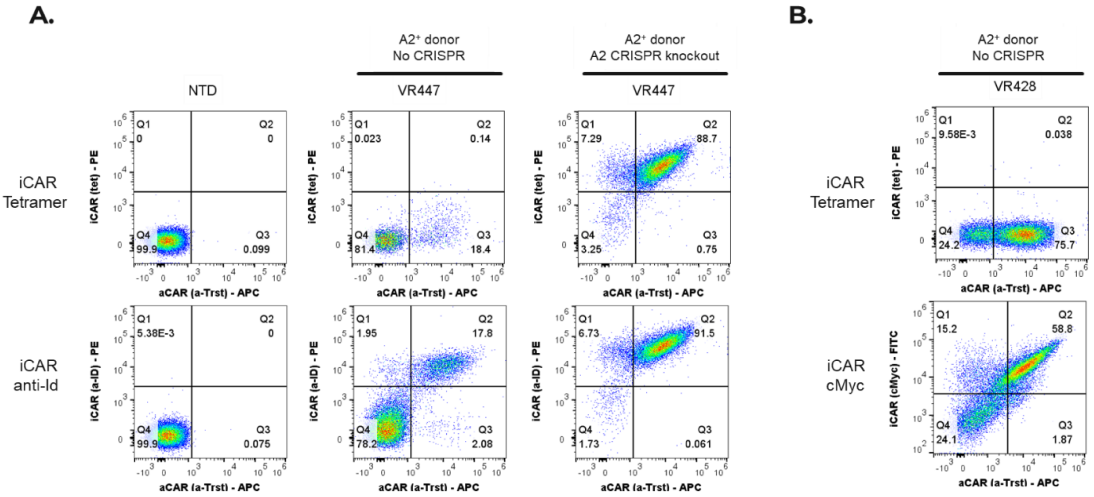

Supplemental Figure S18. *Cis*-inhibition blocks A2 tetramer binding. (A) Tetramer binding analysis. $A2^+$ donor PBMCs were transduced with VR447. The FACS analysis was performed with an A2 tetramer (top panels) or an anti-idiotypic (anti-Id) for huTNG3.2 scFv antibody (lower panels) combined with an anti-Id aCAR-scFv (anti-trastuzumab) to detect CAR expression. The lack of double positive staining with tetramers and detection of NOT gate CAR-T expression with huTNG3.2 scFv anti-Id suggests that the iCAR is blocked by an A2 *cis*-interaction. (B) cMyc tag CAR-T analysis. The experiment shown in (A) was performed in parallel with CAR-T cells generated with a version of VR428 that expresses an N-terminal cMyc-tag (VR518). Detection of the cMyc tagged iCAR with anti cMyc staining indicates that *cis*-inhibition explains the lack of tetramer staining with $A2^+$ donors.

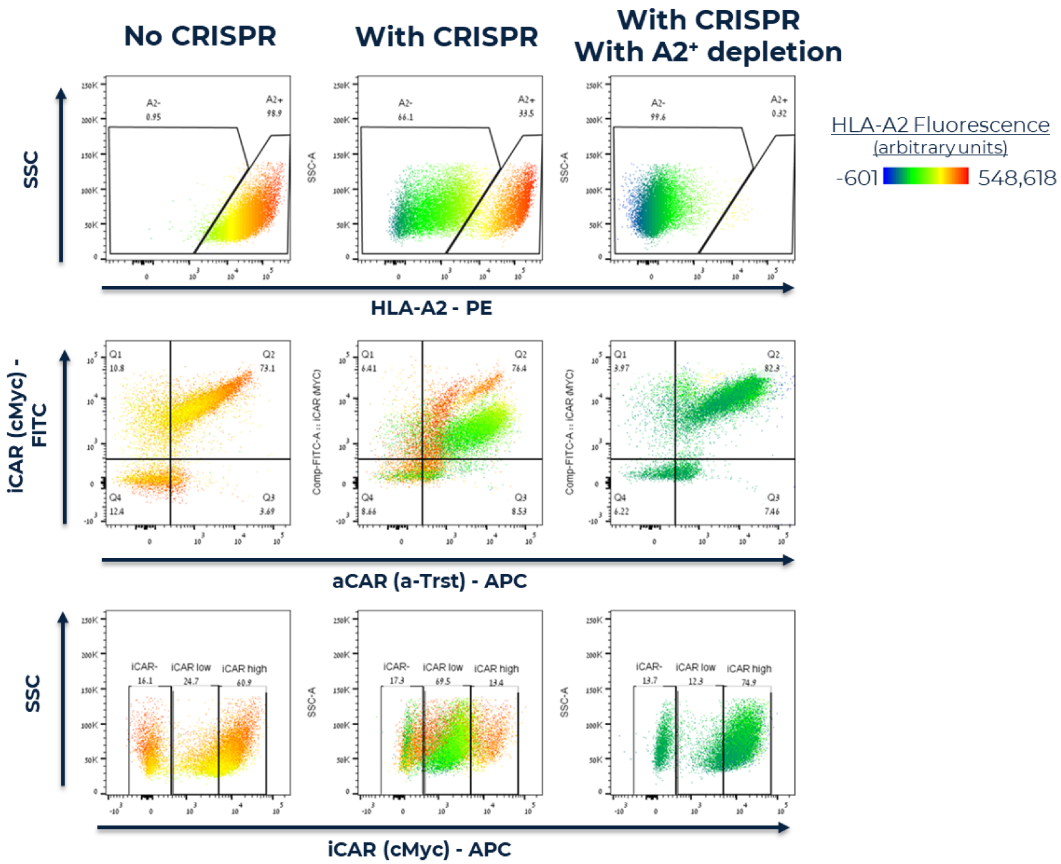

Supplemental Figure S19. FACS analysis of CRISPR edited CAR-T cells. NOT gate CAR-T cells transduced with cMyc-iCAR tagged VR428 were generated with an $A2^+$ donor after CRISPR-editing to knockout A2, with and without A2 depletion**.** The iCAR positive T-cells were enriched by cMyc-FITC bead capture instead of tetramer capture as a final step. Results showed higher levels of iCAR staining in A2 depleted cells. Additional experiments suggest that depletion of residual $A2^+$ cells may not be necessary with more efficient editing (>90%) (data not shown). A2 cell surface expression, and CAR expression were measured by flow cytometry using antibody reagents listed in **online Supplemental Table S1**. Color scale is indicative of the A2 expression level.

Supplemental References:

1. Campbell PJ, Getz G, Korbel JO, Stuart JM, Jennings JL, Stein LD, et al. Pan-cancer analysis of whole genomes. Nature 2020 578:7793 [Internet]. 2020 [cited 2023 May 16];578:82–93. Available from: https://www.nature.com/articles/s41586-020-1969-6

2. Ardlie KG, DeLuca DS, Segrè A V., Sullivan TJ, Young TR, Gelfand ET, et al. The Genotype-Tissue Expression (GTEx) pilot analysis: Multitissue gene regulation in humans. Science (1979) [Internet]. 2015 [cited 2023 May 16];348:648–60. Available from: https://www.science.org/doi/10.1126/science.1262110

3. Ghandi M, Huang FW, Jané-Valbuena J, Kryukov G V., Lo CC, McDonald ER, et al. Next-generation characterization of the Cancer Cell Line Encyclopedia. Nature 2019 569:7757 [Internet]. 2019 [cited 2023 May 16];569:503–8. Available from: https://www.nature.com/articles/s41586-019-1186-3

4. Li J, Zhao W, Akbani R, Liu W, Ju Z, Ling S, et al. Characterization of Human Cancer Cell Lines by Reverse-phase Protein Arrays. Cancer Cell [Internet]. 2017 [cited 2023 May 16];31:225–39. Available from: http://www.cell.com/article/S1535610817300053/fulltext

5. Niepel M, Hafner M, Pace EA, Chung M, Chai DH, Zhou L, et al. Profiles of basal and stimulated receptor signaling networks predict drug response in breast cancer lines. Sci Signal [Internet]. 2013 [cited 2023 May 16];6. Available from: https://www.science.org/doi/10.1126/scisignal.2004379

6. Nusinow DP, Szpyt J, Ghandi M, Rose CM, McDonald ER, Kalocsay M, et al. Quantitative Proteomics of the Cancer Cell Line Encyclopedia. Cell [Internet]. 2020 [cited 2023 May 16];180:387-402.e16. Available from: http://www.cell.com/article/S0092867419313856/fulltext

7. Boegel S, Löwer M, Bukur T, Sahin U, Castle JC. A catalog of HLA type, HLA expression, and neoepitope candidates in human cancer cell lines. Oncoimmunology [Internet]. 2014 [cited 2023 May 16];3. Available from: https://www.tandfonline.com/doi/abs/10.4161/21624011.2014.954893

8. Willcox BE, Thomas LM, Bjorkman PJ. Crystal structure of HLA-A2 bound to LIR-1, a host and viral major histocompatibility complex receptor. Nat Immunol. 2003;4:913–9.